AIP | Applied Physics Letters

Loss-compensated broadband epsilon-near-zero metamaterials with gain media

Lei Sun, Xiaodong Yang, and Jie Gao

Citation: Applied Physics Letters **103**, 201109 (2013); doi: 10.1063/1.4831768
View online: http://dx.doi.org/10.1063/1.4831768
View Table of Contents: http://scitation.aip.org/content/aip/journal/apl/103/20?ver=pdfcov
Published by the AIP Publishing

Loss-compensated broadband epsilon-near-zero metamaterials with gain media

Lei Sun, Xiaodong Yang,[a] and Jie Gao[b]
Department of Mechanical and Aerospace Engineering, Missouri University of Science and Technology, Rolla, Missouri 65409, USA

(Received 14 September 2013; accepted 3 November 2013; published online 13 November 2013)

The concept of loss-compensated broadband epsilon-near-zero metamaterials consisting of step-like metal-dielectric multilayer structures doped with gain media is proposed based on the combination of the Milton representation of the effective permittivity and the optical nonlocality due to the metal-dielectric multilayer structures. With the loss compensation by gain media, broadband epsilon-near-zero metamaterials possesses significantly low material loss in optical frequency range, leading to superior broadband electromagnetic properties for realizing unique functional optical devices, such as the demonstrated prisms for broadband directional emission and S-shaped lenses for phase front shaping. © *2013 AIP Publishing LLC*.
[http://dx.doi.org/10.1063/1.4831768]

Metamaterials with near-zero permittivity (epsilon-near-zero, ENZ) have recently emerged into the focus of extensive exploration due to their anomalous electromagnetic responses and unique functional applications.[1–9] Conventional ENZ metamaterials suffer the disadvantage of the single frequency operation, which is hard to meet the bandwidth requirement in practical applications. Therefore, a strategy has been theoretically studied and numerically demonstrated to construct the broadband ENZ metamaterials[10,11] based on the Bergman spectral representation[12–14] of the effective permittivity. However, such broadband ENZ metamaterials possess a high material loss in the operation frequency range according to the Kramers-Kronig relations,[15] which still limits the practical applications. To overcome such disadvantage, gain media can be incorporated so as to efficiently reduce the material loss in metamaterials.[16] Especially when gain media are used in ENZ metamaterials, high effective optical gain can be achieved due to the strong local field enhancement.[17,18]

In this Letter, a realistic gain-doped broadband ENZ meta-atom in optical frequency range is realized with the step-like meta-dielectric multilayer structures. The developed strategy[19] is carried out based on the Milton representation[20–22] of the effective permittivity in a dimensionless spectral space under quasi-static condition, while the geometric structures of the gain-doped broadband ENZ meta-atom is obtained from the corresponding spectral structures via an inverse problem. Subsequently, the geometric structures are modified according to the optical nonlocality in metal-dielectric multilayer structures based on the transfer matrix method.[23,24] The functional optical devices constructed by the gain-doped broadband ENZ meta-atom are also demonstrated to realize exotic electromagnetic properties with low loss, including the prisms for broadband directional emission and the S-shaped lenses for broadband phase front shaping. These results clearly indicate that the gain-doped broadband ENZ metamaterials possess superior electromagnetic properties for advancing many practical applications.

Depicted in Fig. 1(a), the proposed broadband gain-doped ENZ meta-atom (gain meta-atom) is a two-dimensional three-step multilayer structure with the dimensions of 100 nm × 5 nm and the operation frequency range from 443.702 THz to 489.378 THz. Each step of the gain meta-atom is a metal-dielectric multilayer structure with the dielectric solution doped with gain media. The metallic inclusion is chosen as gold (Au) with the permittivity following the simple Drude model $\varepsilon_m = \varepsilon_\infty - \omega_p^2/(\omega(\omega + i\gamma))$ characterized by the dielectric constant $\varepsilon_\infty = 5.7$, the plasma frequency $\omega_p = 1.3666 \times 10^{16}$ rad/s, and the damping factor $\gamma = 3 \times 4.0715 \times 10^{13}$ rad/s. Note that the damping factor is of the value three times higher than the bulk value in order to account for the surface scattering, the grain boundary effect, and the inhomogeneous broadening of the metallic thin film. The permittivity of the gain-doped dielectric solution follows the simple Lorentz mode:

$$\varepsilon_g = \varepsilon_r + \frac{\sigma_{a1}\Delta N_1}{\omega^2 - \omega_{a1}^2 + i\omega\Delta\omega_{a1}} + \frac{\sigma_{a2}\Delta N_2}{\omega^2 - \omega_{a2}^2 + i\omega\Delta\omega_{a2}}, \quad (1)$$

where the first term ε_r represents the permittivity of the dielectric solution with the value of 2.25, while the following two Lorentz terms (distinguished by the subscript 1 and 2) individually represent the gain effect of two different gain media, the Rhodamine 800 (R800) and the Rhodamine 6G (R6G). In the two Lorentz terms, factor $\sigma_{a1,2}$ represents the coupling strength of the polarization density in the emission band, frequency $\omega_{a1,2}$ represents the center emission frequency, and frequency $\Delta\omega_{a1,2}$ represents the frequency linewidth. Besides, factor $\Delta N_{1,2}$ is related to the energy level decay rates, the gain media concentrations, and the external pumping rate. Associated with the designed operation frequency range, the concentration of R800 and R6G is 0.0263281 mol/l and 0.100416 mol/l, respectively, while the external pumping rate is 6.5×10^9 s^{-1}. The detailed values of other parameters in Eq. (1) are all referred to Ref. 16.

[a]Electronic mail: yangxia@mst.edu
[b]Electronic mail: gaojie@mst.edu

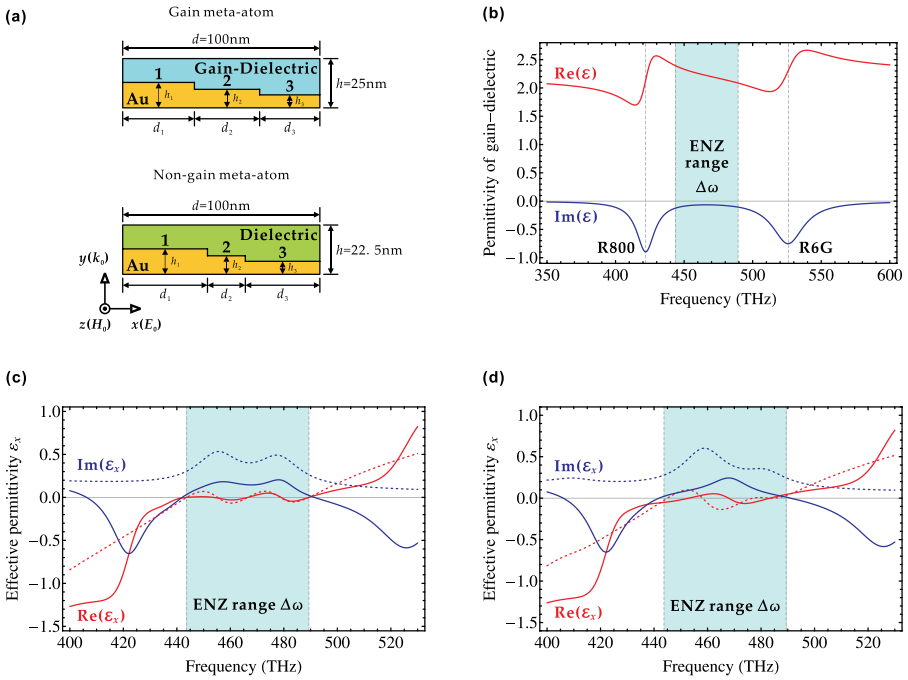

FIG. 1. (a) The schematic diagram of the gain meta-atom, and the non-gain meta-atom, constructed with step-like metal-dielectric multilayer structures. (b) The permittivity of the gain media doped dielectric solution with the light blue area indicating the designed operation frequency range. (c) The values of the effective permittivity of the gain meta-atom (solid curves) and the non-gain meta-atom (dashed curves) based on the Milton representation. (d) The retrieved effective permittivity of the single gain meta-atom (solid curves) and the single non-gain meta-atom (dashed curves).

According to Eq. (1), Fig. 1(b) displays the variation of the permittivity for the gain-doped dielectric solution with respect to the frequency, with the light blue area indicating the designed operation frequency range. The negative imaginary part of the permittivity clearly represents the loss compensation in the gain-doped dielectric solution, while the two resonance peaks of the permittivity imaginary part indicate the center emission frequencies of the two gain media. For comparison, a broadband ENZ meta-atom without gain media (non-gain meta-atom), also composed by Au and dielectric solution (permittivity $\varepsilon_r = 2.25$) with the same operation frequency range, is designed with a similar structure depict in Fig. 1(a).

The broadband ENZ meta-atom is designed properly with the filling ratio of Au inclusion in each step $f_i = h_i/h$ $(i = 1, 2, 3)$ to ensure the zero effective permittivity at the specified frequency in the operation frequency range, and the corresponding thickness of each step d_i $(i = 1, 2, 3)$ to modify the interactions between the adjacent steps, leading to the broadband ENZ response across the operation frequency range. Starting from quasi-static condition, the effective permittivity of the gain meta-atom ε_x reads

$$\varepsilon_x(s) = \varepsilon_g \left(\sum_{i=1}^{3} \frac{d_i/d}{1 - f_i/s} \right)^{-1}, \tag{2}$$

associated with the effective permittivity of each step $\varepsilon_x^{(i)}$ following the simple mixing rule $\varepsilon_x^{(i)} = \varepsilon_g(1 - f_i/s)$. The factor s is defined as $s = s(\omega) = \varepsilon_g/(\varepsilon_g - \varepsilon_m)$, while the factor $d = \sum_{i=1}^{3} d_i$ is the thickness of the gain meta-atom. On the other hand, the effective permittivity ε_x can also be represented by the Milton representation as

$$\varepsilon_x(s) = \varepsilon_g \prod_{i=1}^{3} \frac{s - z_i}{s - s_i}, \tag{3}$$

with respect to a series of pole (s_i) and zero (z_i) pairs confined as $0 \le s_1 < z_1 < s_2 < z_2 < s_3 < z_3 \le 1$. The values of the zeros z_i are defined as $z_i = \mathrm{Re}[s(\omega_i)]$ with three frequencies ω_i equally spaced in the operation frequency range, while the values of the poles s_i are determined as $s_1 = 0$ and $s_i = (z_{i-1} + z_i)/2$ $(i = 2, 3)$. The zero value of the first pole s_1 is because of the simple mixing rule applied on the effective permittivity of each step. The definition of the pole-zero pairs ensures the effective permittivity ε_x exactly equals to zero at all zeros under the lossless condition. Regarding the material loss, the variation on the initial zeros z_i is considered as

$$\mathrm{Re}[\varepsilon_x(s)]_{\omega=\omega_i} = \mathrm{Re}\left[\varepsilon_g \prod_{i=1}^{3} \frac{s - z_i'}{s - s_i} \right] = 0, \tag{4}$$

$(i = 1, 2, 3)$, thus the real part of the effective permittivity ε_x will be equal to zero at all varied zeros z_i'. Finally, the geometric structure $(f_i, d_i/d)$ of the gain meta-atom can be obtained through the following inverse problem:

$$\varepsilon_g \prod_{i=1}^{3} \frac{s - z_i'}{s - s_i} = \varepsilon_g \left(\sum_{i=1}^{3} \frac{d/d_i}{1 - f_i/s} \right)^{-1}, \tag{5}$$

with the results listed in Table I. The above approach is also used to design the non-gain meta-atom with the results in Table II. The corresponding effective permittivity ε_x based on Eq. (2) is also displayed in Fig. 1(c), which clearly demonstrates that the material loss $[\mathrm{Im}(\varepsilon_x)]$ of the gain meta-atom is strongly suppressed due to the loss compensation of the gain media.

TABLE I. Geometric structure of gain meta-atom.

Step	d_i/d	$f_i = h_i/h$	$f_i' = h_i'/h$
1	0.409102	0.129572	0.130701
2	0.247661	0.121897	0.122942
3	0.343238	0.115662	0.116642

TABLE II. Geometric structure of non-gain meta-atom.

Step	d_i/d	$f_i = h_i/h$	$f_i' = h_i'/h$
1	0.438842	0.141011	0.142909
2	0.181592	0.123298	0.124843
3	0.379566	0.107335	0.108573

The above approach is performed under the quasi-static condition, which only considers the filling ratio of the Au inclusions in each step f_i and the thickness of each step d_i/d in the meta-atom, but not includes the realistic dimensions of the metal-dielectric multilayer meta-atom. To improve the accuracy of the design, the optical nonlocality caused by the strong variation of the electromagnetic field on the dimension of metal-dielectric meta-atom needs to be taken into account. The effective permittivity of each step $\varepsilon_x^{(i)}$ should be re-determined as $\varepsilon_x^{(i)} = (k_y^{(i)}/k)^2$ $(i = 1, 2, 3)$ based on the band structure of the metal-dielectric multilayer stack of each step according to the transfer-matrix method as

$$\cos(k_y^{(i)}h) = \cos(k_y^{(m)}h_i')\cos(k_y^{(g)}(h-h_i')) - \frac{1}{2}\left(\frac{\varepsilon_m k_y^{(g)}}{\varepsilon_g k_y^{(m)}} + \frac{\varepsilon_g k_y^{(m)}}{\varepsilon_m k_y^{(g)}}\right)\sin(k_y^{(m)}h_i')\sin(k_y^{(g)}(h-h_i')), \quad (6)$$

with respect to a TM-polarized electromagnetic wave (with non-vanishing component of E_x, E_y, and H_z). Here, the wave vector $k = \omega/c$ and $k_y^{(m,g)} = \sqrt{k^2\varepsilon_{(m,g)} - \left(k_x^{(i)}\right)^2}$, while h_i' represents the revised height of the Au inclusion in each step. The revised height of Au inclusion in each step h_i' is determined from Eq. (6) at the same specified frequencies ω_i where the effective permittivity of each step $\varepsilon_x^{(i)}$ equals to zero with $k_x^{(i)} = 0$, and listed in Tables I and II as $f_i' = h_i'/h$. Based on the realistic dimensions of the meta-atom, the effective permittivity ε_x can be retrieved by numerical simulations using the finite element method (FEM), according to the definition of effective permittivity $\varepsilon_x = \int D_x dV / \int E_x dV$. Figure 1(d) displays the results of the retrieved effective permittivity from single meta-atom, which are almost coincident with the results of the quasi-static design shown in Fig. 1(c), except small perturbations due to the inevitable scattering caused by the internal structures of the meta-atom that is not taken into account in the quasi-static design. It is also worth mentioning that the regions outside the operation frequency range, where the imaginary part of the effective permittivity is negative due to strong loss compensation, suggest the emergence of wave instabilities and amplified spontaneous emission in real experiments.

The loss compensation dramatically suppresses the material loss, leading to superior performance to the gain meta-atom constructed functional optical devices. However, it is worth mentioning that in the functional optical devices constructed by the meta-atoms, the effective permittivity will be slightly different from the single meta-atom due to the optical coupling between adjacent meta-atoms. Figure 2(a) indicates the effective permittivity of the meta-atom array,

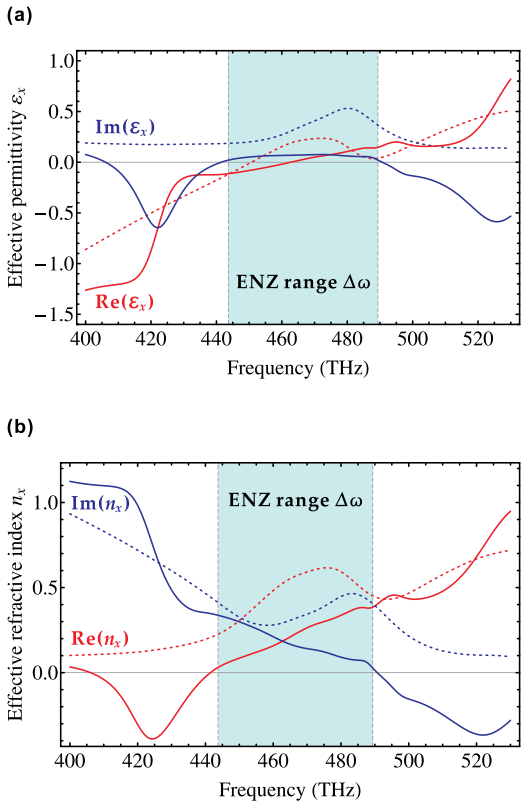

FIG. 2. (a) The retrieved effective permittivity of the gain meta-atom array (solid curves) and the non-gain meta-atom array (dashed curves), constructed by $N_x \times N_y = 5 \times 10$ meta-atoms. (b) The corresponding effective refractive index of the gain meta-atom array (solid curves) and the non-gain meta-atom array (dashed curves).

juxtaposed by $N_x \times N_y = 5 \times 10$ meta-atoms with the total dimensions comparable to the wavelength in free space. It is shown that although the effective permittivity of the meta-atom array is still close to zero in the operation frequency range, the effective permittivity for the meta-atom array has less oscillation compared to Fig. 1(d), because of the interaction among the adjacent meta-atoms. Meanwhile, the material loss of the gain meta-atom array is still greatly less than that of the non-gain meta-atom array. The corresponding effective refractive index for the meta-atom array is also displayed in Fig. 2(b), according to the formula of $n_x = \sqrt{\varepsilon_x}$. It is clear that due to the loss compensation by gain media, both the real part and the imaginary part of the effective refractive index for the gain meta-atom array are much smaller than that of the non-gain meta-atom array in the designed operation frequency range, which will directly lead to superior performance in functional optical devices constructed with the gain meta-atoms.

Figure 3 displays the results from the constructed ENZ prism, made of the meta-atoms with an oblique upper surface of 10° in the air, for realizing broadband directional emission. Figure 3(a) gives the simulation results at the frequency of 464 THz for both the gain prism and the non-gain prism, with a TM-polarized Gaussian beam incident from the bottom of the prism. Compared with the non-gain prism, the angle of refraction of the out-going Gaussian beam is much smaller in the gain prism, while the amplitude of the out-going Gaussian beam from the gain prism is also much stronger because of the loss compensation of the gain media. In

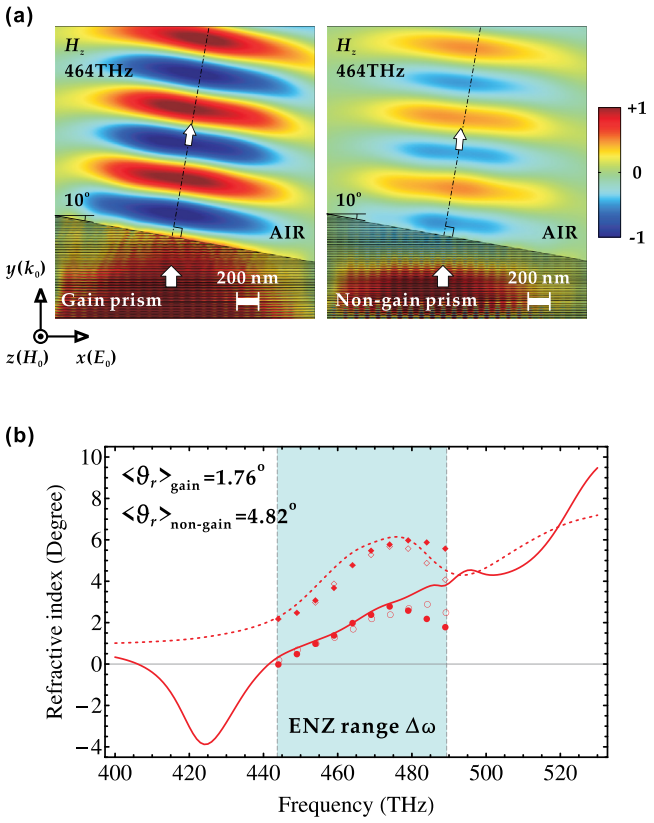

FIG. 3. (a) Simulation results about the directional emission from the gain prism and the non-gain prism with a 10°-oblique upper surface at the frequency of 464 THz, where the distribution of the magnetic field amplitude H_z and the direction of the power flow (hollowed arrows) are shown. (b) The variation of the angle of refraction for the gain prism and the non-gain prism, based on the Snell's law (solid curve and dashed curve), the simulation on the meta-atom constructed prisms (solid circles and solid diamonds), and the simulation on the effective medium constructed prisms (hollowed circles and hollowed diamonds), respectively.

addition, Fig. 3(b) summarizes the variations of the angle of refraction with respect to the frequency for both the gain prism and the non-gain prism. The solid (gain prism) and dashed (non-gain prism) curves represent the angle of refraction calculated from the Snell's law based on the retrieved effective refractive index in Fig. 2(b). On the other hand, numerical simulations are performed at 10 equally spaced frequencies, from 444 THz to 489 THz, in the operation frequency range, with the results marked by the circle (gain prism) and diamond (non-gain prism) symbols. For comparison, simulations are considered for both the meta-atom constructed prism (solid symbols) and the effective medium constructed prism (hollowed symbols) with the retrieved effective permittivity in Fig. 2(a). It is clear that for both gain prism and non-gain prism, the variations of the angle of refraction, calculated from the three methods, are coincident with each other in the operation frequency range. However, for the gain prism, it is still found that the theoretical angle of refraction is different from the simulation results when the frequency approaches to the right boundary of the operation frequency range. That is because the imaginary part of the retrieved effective permittivity of the gain prism becomes negative once the frequency crosses the right boundary of the operation frequency range, indicating that the gain prism has a positive net gain so that the determination of the refractive index does not simply follow the definition of $n_x = \sqrt{\varepsilon_x}$ but becomes more complicated.[25–28] Furthermore, the average value of the angle of refraction of the gain prism is only 1.76°, which is much smaller than 4.82° obtained with the non-gain prism. It indicates clearly that the gain prism presents superior performance in the entire operation frequency range due to the loss compensation of the gain media.

With the near-zero permittivity, the gain (non-gain) meta-atom can also be constructed as S-shaped lenses for shaping the phase front of the electromagnetic wave displayed in Fig. 4. The simulation results shown in Fig. 4(a) are calculated at the frequency of 464 THz for the S-shaped lenses made of gain meta-atoms and non-gain meta-atoms with the same geometry. Clearly, the shape of the phase front of the out-going Gaussian beam from the gain S-shaped lens matches the upper surface geometry much better than that from the non-gain S-shaped lens, due to the smaller refractive index in the gain S-shaped lens. Additionally, Fig. 4(b) summarizes the average phase variation of the out-going Gaussian beam in terms of the theoretical results based on the retrieved effective permittivity, and the simulation results based on the meta-atom constructed S-shaped lenses and the effective medium constructed S-shape lenes for both gain S-shaped lens and non-gain S-shaped lens. It is clear that all these results agree with each other in the designed operation frequency range. However, it is still worth mentioning that

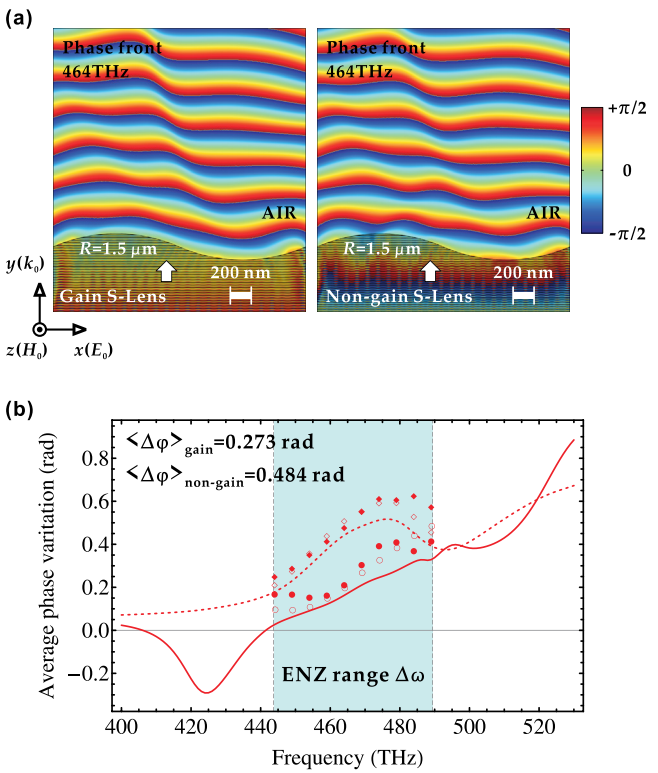

FIG. 4. (a) Simulation results about the phase front shaping from the gain S-shaped lens and the non-gain S-shape lens with the radius of curvature of 1.5 μm, where the distribution of the phase front of the electromagnetic wave is illustrated. (b) The variation of the average phase variation based on the retrieved effective permittivity (solid curve and dashed curve), the simulation results on the meta-atom constructed S-shaped lenses (solid circles and solid diamonds), and effective medium constructed S-shaped lenses (hollowed circles and hollowed diamonds).

due to the inevitable scattering from the internal structures and the boundaries, the simulation results are not exactly the same as the theoretical results. Nevertheless, the apparent difference between mean value of the average phase variation of the gain S-shaped lens (0.273 rad) and the non-gain S-shaped lens (0.484 rad) demonstrates the advantage of the loss compensation by gain media.

In conclusion, based on the Milton representation of the effective permittivity and the optical nonlocality due to the metal-dielectric multilayer structures calculated from the transfer-matrix method, the design strategy for achieving the gain-doped broadband ENZ meta-atom consisting of step-like metal-dielectric multilayer structures in optical frequency range has been proposed and demonstrated. Functional optical devices including prims for directional emission and S-shaped lenses for phase front shaping have been constructed with the gain-doped broadband ENZ meta-atoms to realize exotic broadband electromagnetic properties. Due to the compensation effect of the gain media, the material loss has been significantly reduced so that and the performance of functional optical devices can be improved over the broad operation frequency range. The demonstrated loss-compensated broadband ENZ metamaterials will further enhance many practical applications in optical communications, imaging processing, energy redirecting, and adaptive optics.

This work was partially supported by the Energy Research and Development Center and the Intelligent Systems Center at Missouri S&T, and the University of Missouri Research Board.

[1]S. Enoch, G. Tayeb, P. Sabouroux, N. Guérin, and P. Vincent, Phys. Rev. Lett. **89**, 213902 (2002).
[2]M. Silveirinha and N. Engheta, Phys. Rev. Lett. **97**, 157403 (2006).
[3]A. Alù, M. G. Silveirinha, A. Salandrino, and N. Engheta, Phys. Rev. B **75**, 155410 (2007).
[4]M. G. Silveirinha and N. Engheta, Phys. Rev. B **76**, 245109 (2007).
[5]R. Liu, Q. Cheng, T. Hand, J. J. Mock, T. J. Cui, S. A. Cummer, and D. R. Smith, Phys. Rev. Lett. **100**, 023903 (2008).
[6]B. Edwards, A. Alù, M. E. Young, M. Silveirinha, and N. Engheta, Phys. Rev. Lett. **100**, 033903 (2008).
[7]M. Silveirinha and N. Engheta, Phys. Rev. Lett. **102**, 103902 (2009).
[8]S. Feng, Phys. Rev. Lett. **108**, 193904 (2012).
[9]L. Sun, S. Feng, and X. Yang, Appl. Phys. Lett. **101**, 241101 (2012).
[10]L. Sun and K. W. Yu, J. Opt. Soc. Am. B **29**, 984 (2012).
[11]L. Sun, J. Gao, and X. Yang, Phys. Rev. B **87**, 165134 (2013).
[12]D. J. Bergman, Phys. Rep. **43**, 377 (1978).
[13]D. J. Bergman, Phys. Rev. B **19**, 2359 (1979).
[14]D. J. Bergman and D. Stroud, Solid State Phys. **46**, 147 (1992).
[15]J. S. Toll, Phys. Rev. **104**, 1760 (1956).
[16]S. Campione, M. Albani, and F. Capolino, Opt. Mater. Express **1**, 1077 (2011).
[17]D. J. Bergman and M. I. Stockman, Phys. Rev. Lett. **90**, 027402 (2003).
[18]M. I. Stockman, Nat. Photonics **2**, 327 (2008).
[19]L. Sun and K. W. Yu, Appl. Phys. Lett. **100**, 261903 (2012).
[20]G. W. Milton, Appl. Phys. Lett. **37**, 300 (1980).
[21]G. W. Milton, J. Appl. Phys. **52**, 5286 (1981).
[22]G. W. Milton, J. Appl. Phys. **52**, 5294 (1981).
[23]J. Elser, V. A. Podolskiy, I. Salakhutdinov, and I. Avrutsky, Appl. Phys. Lett. **90**, 191109 (2007).
[24]A. V. Chebykin, A. A. Orlov, C. R. Simovski, Yu. S. Kivshar, and P. A. Belov, Phys. Rev. B **86**, 115420 (2012).
[25]Y.-F. Chen, P. Fischer, and F. W. Wis, Phys. Rev. Lett. **95**, 067402 (2005).
[26]J. Skaar, Phys. Rev. E **73**, 026605 (2006).
[27]A. A. Govyadinov, V. A. Podolskiy, and M. A. Noginov, Appl. Phys. Lett. **91**, 191103 (2007).
[28]B. Nistad and J. Skaar, Phys. Rev. E **78**, 036603 (2008).